

# A Transferable and Automatic Tuning of Deep Reinforcement Learning for Cost Effective Phishing Detection

Orel Lavie, Asaf Shabtai, Gilad Katz

*Department of Software and Information Systems Engineering  
Ben-Gurion University of the Negev  
Be'er Sheva, Israel*

---

## Abstract

Many challenging real-world problems require the deployment of ensembles—multiple complementary learning models—to reach acceptable performance levels. While effective, applying the entire ensemble to every sample is costly and often unnecessary. Deep Reinforcement Learning (DRL) offers a cost-effective alternative, where detectors are dynamically chosen based on the output of their predecessors, with their usefulness weighted against their computational cost. Despite their potential, DRL-based solutions are not widely used in this capacity, partly due to the difficulties in configuring the reward function for each new task, the unpredictable reactions of the DRL agent to changes in the data, and the inability to use common performance metrics (e.g., TPR/FPR) to guide the algorithm’s performance. In this study we propose methods for fine-tuning and calibrating DRL-based policies so that they can meet multiple performance goals. Moreover, we present a method for transferring effective security policies from one dataset to another. Finally, we demonstrate that our approach is highly robust against adversarial attacks.

*Keywords:* Phishing detection, Machine learning, Deep reinforcement learning

---

---

\*Corresponding author.

*Email addresses:* orella@post.bgu.ac.il (Orel Lavie), shabtaia@bgu.ac.il (Asaf Shabtai), giladkz@bgu.ac.il (Gilad Katz)

## 1. INTRODUCTION

Ensembles are a common approach to improving the performance of machine learning algorithms. Instead of relying on a single algorithm, ensembles combine the output of several learning models to obtain a more accurate result. Ensembles are commonly used not only to improve classification or regression performance [1, 2, 3], but also to create solutions that are more robust against noise [4, 5] and adversarial examples [6, 7].

While the advantages of using ensembles are considerable, they are not without drawbacks. First, running ensembles can be computationally costly because of the need to train and apply multiple learning models prior to producing a classification. Secondly, while the individual learning models of the ensemble can usually be run in parallel, they all need to conclude their processing of the analyzed data before the ensemble can produce its output. These two drawbacks are particularly challenging in domains where ensembles consist both of a large number of learning models, with large variance in the running times of the individual models. In such cases, the processing of an item may be delayed for a long period of time due to a single model out of dozens.

The aforementioned drawbacks make clear the need for a more refined solution, that can weigh the benefit of using each individual learning model in an ensemble against its cost (measured by running time, computing cost, etc.). Such an elegant solution to this problem was recently proposed in [8], where the authors presented SPIREL, a deep reinforcement learning (DRL) framework for the dynamic sequential allocation of detectors for each sample. Based on the scores assigned by previous detectors, SPIREL either allocates additional detectors or produces a classification. SPIREL’s reward function assigns a value to correct/incorrect classifications, as well as to the runtime required to analyze each sample. SPIREL was evaluated on malware detection in executable and Android files, and was able to reduce running time by 80% while reducing the accuracy and F1 metrics by just 0.5%.

While effective, SPIREL suffers from two limitations that make it difficult

to apply in real world scenarios. First, *SPIREL lacks the (basic) capability of supervised learning algorithms to operate on predefined true positive (TP)/false positive (FP) goals*. This ability is critical, as organizations often define these thresholds so that their day-to-day operations are not disturbed. In standard supervised learning solutions, organizations that experience too many false alarms would simply increase the confidence score threshold required to identify a sample as malicious, without re-training their models. Doing the same for SPIREL, however, would require modifying the reward function and retraining the model.

SPIREL’s second limitation, which exacerbates the first, is the *difficulty of achieving and maintaining the desired levels of TP/FP rates*. The DRL-agent’s reward function, which guides its decision making process, assigns positive and negative rewards for correct and incorrect classifications, respectively. The size of these rewards determines SPIREL’s policy. However, this reward structure is a blunt instrument, and small changes to the reward structure can have a non-linear impact on an agent’s behavior. Therefore, fine-tuning a DRL agent for specific desired detection levels is difficult and requires multiple runs and delicate optimization. Even worse, changes in the data—a common phenomenon in real life—would require performing the tuning process yet again.

In this study we propose CETRA, a novel approach for dynamically adapting DRL-based methods to achieve and maintain desired levels of performance. CETRA enables organizations to first define desired values for their key performance indicators (e.g., AUC, RAM usage, running time), and then dynamically modifies its reward function to meet these goals. This capability alleviates one of the main difficulties in applying DRL to real-world applications: the configuration of the model. To further enhance CETRA’s ability to adapt to organizational policy, we present a probability density-based measure that enables us to translate a successful configuration from one domain to another. Finally, we demonstrate that our approach is highly robust against adversarial attacks.

We evaluate CETRA on two phishing detection datasets, and demonstrate CETRA ability to offer a highly cost-effective solution: our derived security policy reduces the processing time by as much as 76% with a negative impact

of only 0.25%-0.35% on the F1 metric. Additionally, we demonstrate how a simple definition of goals for metric values can automatically modify the derived security policy to achieve these desired goals, and we demonstrate how our proposed density-based measure can successfully transplant an effective security policy from another domain. Finally, we evaluate the robustness of CETRA to both evasion and resource utilization adversarial machine learning attacks.

To summarize, our contributions are as follows:

- We propose a novel approach for configuring the reward function of DRL-based models. Our approach enables us to define desired values for various metrics—TPR/FPR, RAM usage, etc.—and have the DRL model automatically adapt its behavior in order to reach them.
- We propose a process for “transferring” effective policies from one domain to another. CETRA is therefore able to automatically and efficiently configure our DRL-based approach.
- Finally, we demonstrate that our proposed approach is highly robust against adaptive adversarial attacks.

## 2. RELATED WORK

### 2.1. Phishing Detection Methods

Earlier works in phishing detection involved the use of blacklisting—a repository of web pages known to be malicious. Such solutions include Google’s Safe Browsing and PhishTank services. The main weakness of this approach lies in its inability to defend against unknown websites. As a result, machine learning is the primary tool used nowadays to fight phishing.

Machine learning-based approaches extract various features from the content of the web page or its metadata to classify a given page as benign or phishing. The solutions in this field are numerous and diverse [9, 10, 11, 12, 13, 14]. Zhang et al. [15], for example, used an extreme learning machine (ELM) technique and extracted hybrid features from the page’s URL and text. Recently, due

to their ability to process large amounts of data and learn complex patterns, deep learning (DL) models were proposed for the detection of phishing websites. These methods mainly analyze the URL string using LSTM [16] or CNN [17, 18, 19] models.

## 2.2. Reinforcement Learning

Reinforcement learning (RL) is an area of ML that addresses complex multi-step decision-making processes. These algorithms have been shown to perform well even with noisy and partial information [20]. An RL algorithm normally consists of an agent that interacts with an environment in a sequence of actions and rewards. In each time step  $t$ , the agent selects an action  $a_i \in A = \{a_1, a_2, \dots, a_k\}$ . As a result of  $a_i$ , the agent transitions from the current state  $s_t$  to a new state  $s_{t+1}$ . Additionally, the selection of the action may yield a reward  $r_t$ , which can be either positive or negative. The goal of the agent in each state is to interact with the environment in a way that maximizes the sum of future rewards  $R_T$ :

$$R_T = \sum_{t=1}^T r_t \quad (1)$$

where  $T$  is the terminal (final) step in the sequence.

The selection of actions is made by the policy  $\pi(a, s)$ , which produces the probability of taking action  $a \in A$  when in state  $s \in S$ . A common approach for evaluating the future rewards of an action is by its Q-function, denoted by  $Q(s, a)$ , which calculates the expected reward  $E[R_t | s_t = s, a_t = a, \pi]$ , derived from the pair  $s, a$  for policy  $\pi$  at time  $t$ . In problems consisting of very large state and/or action spaces, estimating  $Q(s, a)$  for every possible state-action combination is infeasible. Therefore, it is common to use an approximation-based solution, such as a neural network. Instead of  $Q(s, a)$ , we use  $Q(s, a; \theta)$ , where  $\theta$  reflects the parameters of the neural network, making it a deep reinforcement learning (DRL) setup [21, 22].

DRL-based algorithms have several properties that make them highly suitable for the security domain. First, they have the capability of efficiently ex-

ploring large state and action spaces [23], and of devising strategies to address complex problems [24]. Additional properties that make DRL useful in security-related scenarios is their ability to operate with partial [20] and noisy information [25]. Finally, their use of the reward function to shape the policy of the algorithm enables the reconciliation of multiple (sometimes conflicting) objectives [8].

### *2.3. Reinforcement Learning-Based Security*

The sequential decision making employed by DRL algorithms make them highly suitable for the development of security policies. Blount et al. [26] presented a proof of concept for an adaptive rule-based malware detection framework for portable executable (PE) files that employs a classifier combined with a rule-based expert system. Then, an RL algorithm is used to determine whether a PE is malicious. Birman et al. [8] proposed a DRL framework for the dynamic sequential allocation of detectors for each sample. Based on the scores assigned by previous detectors, their framework either allocates additional detectors or produces a classification. In the field of email phishing detection, Smadi et al. [27] proposed a two-mode framework. In the online mode, the framework employs a DRL agent to detect phishing attacks. Offline, the model adapts to changing circumstances by performing additional learning.

Fu et al. [28] introduced adversarial inverse reinforcement learning (AIRL), a practical and scalable inverse RL algorithm based on an adversarial reward learning formulation. Another work in the field of adversarial learning by Anderson et al. [29] presented a reinforcement learning method that learns which sequences of operations are likely to enable a sample to avoid detection. Recently, Mo et al. [30] introduced Decoupled Adversarial Policy, which uses two sub-policies: one that determines when to launch an attack, and another that determines what actions the model should be “lured” into taking.

### 3. PROPOSED METHOD

CETRA builds upon the work of Birman et al. [8], which proposed SPIREL, a DRL-based approach for the efficient utilization of ensembles: rather than deploy all detectors at once, the agent dynamically select which additional detectors (if any) to call based on the results of previous ones. While highly effective, SPIREL is hindered by its inability to adapt its policy to achieve specific performance metric goals (e.g., false-positive rate of no more than 1%), or to easily keep these metrics stable in the face of changing data. In this section we present our proposed solution to these limitations.

This section consists of two parts: in Section 3.1, we present the basic building blocks of our approach: states, actions, and preliminary reward function. In Section 3.2 we present our proposed expansions, which address the multiple limitations that complicate the deployment of DRL-based solutions to real-world scenarios.

#### 3.1. Base Method

In this section we present the states, actions, and rewards representation of our proposed approach. Our representation closely follows that of [8], as we build upon this base in the following section.

**States.** Our state space consists of all possible combinations of detector outputs. Therefore, for a given set of detectors  $D$ , we represent each state  $s \in S$  using a vector of size  $|s| = |D|$ . Each entry in the vector represents the output produced by its corresponding detector, which can be considered as the certainty level—the degree to which the detector is certain of the web page’s maliciousness. For yet-to-be-activated detectors we use a default value of -1:

$$v_i = \begin{cases} [0, 1] & , \text{detector prediction, if used} \\ -1 & , \text{otherwise} \end{cases} \quad (2)$$

**Actions.** Our action space consists of two types of actions: *detector activation* and *classification*. The former is used to apply one detector on the analyzed web page, so the number of such actions is equal to the number of detectors  $|D|$ . The latter action type is used to issue a final classification for the analyzed web page: either “phishing” or “benign”. Applying either of their final classifications also terminates the analysis of the web page.

**Rewards.** The reward function shapes the DRL agent’s policy. Once our approach classifies a web page, there are four possible outcomes: true positive/negative (TP and TN) and false positive/negative (FP and FN). The *base reward function* used by our approach (as well as SPIREL) is as follows:

$$C_{1_{total}}(T) = \begin{cases} r & , \text{TP or TN} \\ -1 * \sum_{t=1}^T C_1(t) & , \text{FP or FN} \end{cases} \quad (3)$$

where  $r$  is a constant and  $C_1(t)$  is a time-dependent loss function that the “punishment” it assigns to the DRL is proportional to the amount of computing resources spent on the classification:

$$C_1(t) = \begin{cases} t & , 0 \leq t < 1 \\ 1 + \log_2(\min(t, t_1(s))) & , 1 \leq t \end{cases} \quad (4)$$

The rationale of the approach is straightforward: a fixed reward for correct classifications means that detectors that can provide additional information (i.e., increase certainty) are likely to be used. However, the risk of being mistaken will prevent the DRL-agent from calling upon detectors that provide little to no information, because their use will only incur a larger loss in case of a mistake.

**Limitations of the base method.** While this approach performed well in simulation [8], we identify two significant shortcomings to this approach when applied to real-world use-cases:



1. **Lack of theoretical or practical guidelines** – SPIREL does not offer any method for configuring the  $r$  and  $C_1(t)$ . This makes the approach difficult and computationally costly to implement for new datasets.
2. **The need to conform with multiple objectives** – organizations often define multiple metrics for detection frameworks (e.g., TPR and running time). Manually configuring the reward function—the only level offered by SPIREL—to meet these goals can be computationally prohibitive because of the large search space.

In the next section we present our proposed approach for addressing these challenges.

### 3.2. CETRA

This section comprises three parts. In section 3.2.1 we develop a theoretic foundation for the required traits of an effective multi-objective reward function. In Section 3.2.2, we present our novel approach for reformulating the reward function in a way that enables our DRL-agent to automatically adapt its behavior to comply with multiple objectives without any need for additional calibration. Finally, in Section 3.2.3 we present a novel method for “importing” the settings of one successfully deployed DRL-agent to another.

#### 3.2.1. Theoretical analysis of the cost function

We now formally define guidelines for the design of the reward function used by our approach. Such a definition is important for several reasons. First, such guidelines will produce reward functions with stable and predictable outputs that will facilitate the convergence of the DRL model. Secondly, our guidelines provide a simple framework for the representation of multiple factors (e.g., performance, runtime, RAM usage) in a single reward function, thus making our approach applicable to multiple use-cases and domains. Thirdly, reward functions created using our guidelines can be adapted to new domains, thus preventing exhaustive exploration of the reward function for new domains. Our guidelines are as follows:

- 1) **Consistent reward structure** – “good” and “bad” outcomes will receive positive and negative values, accordingly.
- 2) **Weak monotonous function** – for every outcome, the cost should not decrease as a function of the invested time and/or resources.
- 3) **Bounded on both axes** – the reward function should be bounded on all axes to prevent outliers and noisy data from having an out-sized effect on the DRL agent.
- 4) **Continuous and proportional** – To prevent small changes in the input (e.g., running time) from triggering large fluctuations in the reward function values, we require that the latter be continuous. Moreover, we require the reward function to be a *linear or a super-linear* expression of the input. This setup enables us to increase/decrease the change rate of the reward, thus enabling organizations to define different priorities to different ranges of values (e.g., low/high computational cost for the analysis of a sample). While different priorities can be defined, the linear change rate keeps the change gradual and predictable.

### 3.2.2. Metric Goal-driven Cost Functions

As explained in Section 1, the two main challenges not addressed in SPIREL were *a)* the need to automatically adapt the reward function to obtain the organization’s detection objectives (e.g., TPR/FPR), and; *b)* to smoothly adapt the reward function to changes in the dataset’s characteristics over time, so that the aforementioned goals are maintained. We now describe three modifications to the base approach, designed to overcome these challenges.

**Step 1: reformulation of the different regions, defined by the reward function.** Let  $PR(a \leq x \leq b)$  be the probability density function for the computational cost of the processing samples from a given dataset  $D$ . We define the computational cost of a sample as the cost of analyzing it using all its assigned detectors. The cost can be defined by the organization, and include multiple factors—running time, cloud credits usage, etc.—but in order to make our results comparable to previous work [8], we use running time as a metric.

By considering running time as our cost approximator, the probability density function enables us to obtain the percentage of samples whose processing time is between  $[a, b]$ .

Our proposed representation has two significant advantages. First, it enables the creation of dynamic boundaries that can be automatically adapted to changes in the dataset over time. We are therefore able to define different cost functions to different percentiles of samples, something that was not possible while using the rigid boundaries proposed by [8]. Secondly, this representation provides the theoretical foundation that enables the “translation” of successful policies from one domain to another (see Section 3.2.3).

Without loss of generality, we assume our reward function to have two ‘regions’, each with a different reward slope. The new function (Equation 6) will now form the base for our additional modifications.

$$C_{2_{total}}(T) \begin{cases} r & , \text{TP or TN} \\ -1 * \sum_{t=1}^T C_2(t) & , \text{FP or FN} \end{cases} \quad (5)$$

where  $r$  is a constant and  $C_2(t)$  is defined as follows:

$$C_2(t) = \begin{cases} \frac{t}{d_2} & , 0 \leq t < d_2 \\ 1 + \log_2 \left( \frac{\min(t, t_2(s))}{d_2} \right) & , d_2 \leq t \end{cases} \quad (6)$$

**Step 2: incorporating organizational priorities into the reward function.** As explained earlier, one of SPIREL’s main shortcomings is its inability to incorporate metrics—accuracy, TPR/FPR etc.—into the reward function. We now present a new reward function that achieves this goal:

$$C_{2_{metric}}(m) = \begin{cases} -b * CR(M) & , m < l \\ CR(M) & , l \leq m < u \\ b * CR(M) & , u \leq m \end{cases} \quad (7)$$

where  $u$  and  $l$  are the upper and lower bounds of the acceptable range of the

evaluated metric, and  $m$  is the value obtained by our approach for a batch of  $M$  samples. The parameter  $b$  is a manually defined bonus/penalty factor, and  $CR(M)$  is defined as follows:

$$CR(M) = \sum_{i=1}^M C_{2_{total}}(T_i) \quad (8)$$

where  $\{T_i\}_{i=1}^M$  are the terminal steps for the last  $M$  samples.

The rationale of equation 7 is as follows: if the reward function  $C_{2_{total}}$  yields results that are within the organization’s desired range, the reward is unchanged. If, however, the results are below the predefined range (i.e.,  $m < l$ ), then  $CR(M)$  is significantly reduced. On the other hand, performance that is above the desired range will be rewarded by a bonus. This reward setting is designed so that the DRL-agent’s first priority will be meeting or surpassing the organization’s predefined goal, since achieving this goal is crucial for obtaining high rewards. Once this goal has been achieved, the DRL-agent will turn its attention to optimizing  $CR(M)$ , since any increase in the output of this function will result in a linear or super-linear increase in the value of  $C_{2_{metric}}$ .

**Step 3: Measuring organizational metrics over batches.** While logical, a simplistic implementation of the modification proposed in step 2 is not practical. The reason is that for many metrics—TPR and FPR are two clear examples—we would need to process all the samples in the training set before calculating  $C_{2_{metric}}$  and updating the weights of our neural net. This would significantly slow our model’s convergence.

Our third and final modification to the reward function is the calculation of the  $C_{2_{metric}}$  reward function over *batches*. For each of the analyzed batches of samples in the training phase, we calculate  $CR(M)$  and then determine, according to the value of  $m$  calculated for the said batch, how  $CR(M)$  should be modified. While this approach inevitably injects some volatility into the DRL-agent’s learning, this volatility is balanced out over a large number of batches. As an additional smoothing mechanism, we ensure that the batches are randomly re-sampled at every epoch. As shown by our evaluation, this

approach is effective in enabling CETRA to converge to an effective detection policy.

### 3.2.3. Density Function-based Security Policy Transfer

In the previous section, we described how the reward function of our approach can be designed so that it reflects both the *actual costs of classification* on the one hand, and the *organization’s performance goals* on the other. We now seek to make our approach transferable, by enabling the sharing of successful policies across multiple domains.

While their metrics (e.g., TPR/FPR) may vary, organizations are likely to find it more difficult to quantify the cost of a false classification as a function of resource use, as defined in equation 5. We therefore propose an approach that enables the transfer of effective settings to a new dataset. Please note that while we define our approach as one that operates across datasets, it can also be used to re-calibrate the cost function in cases of data and concept drift.

As defined in Section 3.2.2, the boundaries of the cost function are defined using a probability density function. Let  $C_n$  be the cost function of the dataset  $D_n$ . That is, we define two instances of equation 6 with specific values of  $t$  and  $s$  (i.e., a chosen time percentile). Next we define a continuous random variable  $X_n$  with the probability density function (i.e., PDF) as:

$$f_{X_n}(t) = \begin{cases} \frac{C_n(t)}{k_n} & , 0 \leq t \leq t_n(s) \\ 0 & , \text{otherwise} \end{cases} \quad (9)$$

where  $k_n$  is defined as:

$$k_n = \int_0^{t_n(s)} C_n(t) dt \quad (10)$$

Equation 10, enables us to ensure that the properties of  $f_{X_n}(t)$  are those of a PDF. Next we define a discrete random variable  $Y_n$ , an indicator function of

$X_n$  on a subset  $A = [d_n, t_n(s)]$  as:

$$Y_n = \mathbf{1}_A(X_n) = \begin{cases} 1 & , X_n \in A \\ 0 & , X_n \notin A \end{cases} \quad (11)$$

This indicator is used to determine whether  $X_n$  is below (i.e.,  $Y_n = 0$ ) or above (i.e.,  $Y_n = 1$ ) the threshold. Because  $Y_n$  is a discrete random variable, we can create a vectorized representation of the probability mass function  $P_{Y_n}$  of  $Y_n$  as:

$$P_{Y_n} = [\mathbb{P}(Y_n = 0), \mathbb{P}(Y_n = 1)] \quad (12)$$

where  $\mathbb{P}(Y_n = 0)$  and  $\mathbb{P}(Y_n = 1)$  are defined as:

$$\mathbb{P}(Y_n = 0) = \int_0^{d_n} f_{X_n}(t)dt \quad \mathbb{P}(Y_n = 1) = \int_{d_n}^{t_n(s)} f_{X_n}(t)dt \quad (13)$$

Based on equation 12 and the definition of probability, we derive the following:

$$\mathbb{P}(Y_n = 0) + \mathbb{P}(Y_n = 1) = 1 \quad (14)$$

Based on equation 12 and equation 13, we define a likelihood ratio (i.e., a ratio between the density of lower and higher resources)  $\beta_n$  as:

$$\beta_n = \frac{\mathbb{P}(Y_n = 1)}{\mathbb{P}(Y_n = 0)} = \frac{\int_{d_n}^{t_n(s)} f_{X_n}(t)dt}{\int_0^{d_n} f_{X_n}(t)dt} = \frac{\int_{d_n}^{t_n(s)} C_n(t)dt}{\int_0^{d_n} C_n(t)dt} \quad (15)$$

Based on equations 14 and 15, we derive the following:

$$\mathbb{P}(Y_n = 1) = \frac{\beta_n}{\beta_n + 1} \quad \mathbb{P}(Y_n = 0) = \frac{1}{\beta_n + 1} \quad (16)$$

Let  $n = n_1$  and  $n = n_2$  for datasets  $D_{n_1}$  and  $D_{n_2}$ , respectively. The Kullback–Leibler (i.e., KL) divergence [31] between  $Y_{n_1}$  and  $Y_{n_2}$  for  $n_1 \neq n_2$  is

defined as:

$$D_{KL}(Y_{n_1} \| Y_{n_2}) = \sum_{y=0}^1 \mathbb{P}(Y_{n_1} = y) \log_{10} \left( \frac{\mathbb{P}(Y_{n_1} = y)}{\mathbb{P}(Y_{n_2} = y)} \right) \quad (17)$$

Using equations 16 and 17, we derive the following:

$$\begin{aligned} D_{KL}(Y_{n_1} \| Y_{n_2}) &= \sum_{y=0}^1 \mathbb{P}(Y_{n_1} = y) \log_{10} \left( \frac{\mathbb{P}(Y_{n_1} = y)}{\mathbb{P}(Y_{n_2} = y)} \right) = \\ &= \log_{10} \left( \frac{\beta_{n_2} + 1}{\beta_{n_1} + 1} \right) + \frac{\beta_{n_1}}{\beta_{n_1} + 1} \log_{10} \left( \frac{\beta_{n_1}}{\beta_{n_2}} \right) \end{aligned} \quad (18)$$

To require that the density of  $D_{n_2}$  is similar to  $D_{n_1}$ , and since the KL metric is not symmetrical [32], we require that:

$$0 < \frac{D_{KL}(Y_{n_1} \| Y_{n_2}) + D_{KL}(Y_{n_2} \| Y_{n_1})}{2} < \varepsilon \quad (19)$$

where  $\varepsilon$  is a hyper-parameter tolerance that decides how much the distributions could differ.

In a use-case where  $C_{n_1}$  and  $d_{n_1}$  are known, the above equations enable us to calculate the values of  $\beta_{n_2}$  and  $d_{n_2}$ , and to derive the value of  $C_{n_2}$  that will enable us to achieve comparable performance. This holds true even if the sample distribution of the two datasets, as well as their costs, are different.

The method is further discussed over Appendix D, and the full algorithm is also provided there.

## 4. EXPERIMENTAL SETUP

### 4.1. Datasets

Our evaluation was conducted on two datasets, which we name based on the studies that presented them. The first dataset is *Bahnsen* [16], which contains 1.2M benign URLs taken from the Common Crawl corpus, and 1.146M phishing URLs from PhishTank. The second dataset is *Wang* [19], which contains 245K phishing URLs collected from PhishTank, and 245K benign URLs collected by

searching via different search engines in domains belonging to Alexa 1M ranking URLs, and returning the URLs of the top ten search results.

Because we employ a content-based detector in our experiments, we filtered any URL that could not be reached or lost its phishing activity at the time of our evaluation. Consequently, the Bahnsen dataset was reduced to 687,176 samples overall—354,770 benign and 332,406 phishing. Similarly, the Wang dataset was reduced to 327,646 samples—214,034 benign and 113,612 phishing.

#### 4.2. The Detectors

Our selection of the detectors was guided by two objectives:

**1) Variance in resource consumption.** To demonstrate CETRA’s cost-effectiveness in dynamic detectors selection, the detectors need to have different resource consumption (e.g., runtime) costs.

**2) Detection methods diversity.** To ensure that our detectors have a diverse set of capabilities (and to better model a real-world detection framework), we chose detectors that use various phishing detection methods (e.g., string based and content based).

Based on the aforementioned objectives, we chose to include *five detectors* in our evaluation, all based on studies from recent years.

**CURNN** [16]. This detector directly analyzes the URL’s character sequence. Each characters sequence exhibits correlations with other characters in the sequence, and its underlying assumption is that these correlations could be leveraged for the identification of phishing. We use the implementation described in [16], which uses a standard LSTM architecture.

**eXpose** [17]. This detector receives as input multiple unprocessed string-representing URLs, registry keys etc. These inputs are projected into an embedding layer and then processed using convolutional layers, and finally fed to a dense layer that classifies each sample using a softmax function as phishing or benign.

**PDRCNN** [19]. Encodes the URL as a two-dimensional tensor, and feeds it into a bidirectional LSTM network. The LSTM extracts a representation



for each character in the URL, which is then provided as input to a convolutional architecture that identifies the key characters required for the detection of phishing.

**FFNN** This content-based detector utilizes the 17 features presented in [14] and the 12 features presented in [33]. Both studies extract features from the URL string itself and the content of the page (e.g., external and internal hyperlinks ,etc). Based on these two studies, we used a dense architecture with ten layers.

**XGBoost** [34]. This popular and highly-effective tree-ensemble algorithm applies both boosting and gradient descent. We used five Markov Chain-based models to extract features that are then used as input. Our Markovian models were applied on the 1M Alexa rank dataset as follows: Alexa 1M domain uni-gram, Alexa URL uni-gram, Alexa URL parts (i.e., tld, domains and sub-domains), Alexa URL bi-gram and DNS URL bi-gram.

While the selection of diverse detection methods is important for an ensemble solution, diversity alone is not sufficient. A comprehensive analysis is performed in Appendix A shows that our chosen detectors are complementary, and that no detector dominates another (i.e., achieves equal or better results for all samples).

### *4.3. Experimental Setting*

We ran each detector as an isolated process on a dedicated and identical machine to ensure that the analysis is unbiased. We used a train/validation/test split of 75%/10%/15%. Our proposed framework was implemented using Python v3.8 and OpenAI Gym [35]. We used the actor-critic with experience replay (ACER) [36] (an offline learning DRL algorithm) as our DRL-agent, and used ChainerRL [37] for the implementation. We used an Intel Xeon CPU E5-2690 v4 with 6 cores, 56GB of RAM, and 340GB of SSD disk space.

We set the size of the replay buffer to 5,000, and begin using it in the training process after 100 episodes. Both the policy and action-value networks of the ACER consist of the following architecture: input layer of size 5 (the state vector’s size), a hidden layer of size 32, and an output layer of size 7 (we

have seven possible actions: five individual detector selections, and two final classifications). All layers except for the output layer use the ReLU activation function, while the output layer uses softmax. We set our initial learning rate to 0.001, with an exponential decay rate of 0.99 and  $\epsilon = 1e-8$ . The chosen optimizer was RMSPropAsync, which was shown to perform well for DRL tasks [38]. For the overall evaluation, we use the precision and recall measures, as well as the  $F1$  measure, which is a combination of the two [39].

#### 4.4. The Evaluated Baselines

We compare CETRA to two baselines:

**SPIREL** [8]. The original approach for cost-effective ensemble classification, described in Section 3.1. Given that our proposed novelties build upon this approach, a comparison is called-for.

**Detector combinations.** Because CETRA is based on the intelligent and dynamic deployment of detectors, it is important that we show that no static combination of the detectors (or a subset of them) can outperform our proposed approach. For this reason, we evaluate *every possible detector combination*. We also use four methods for aggregating the classification results of the evaluated detectors: *a)* majority voting – the averaging of the confidence scores of all participating detectors; *b)* the “or” approach, which returns the maximal score from all applied detectors; *c)* stacking – we feed all the confidence scores into Random Forest and Decision Tree algorithms, and use them to produce the final confidence scores, and; *d)* boosting – we use Adaboost algorithm to produce final scores. Overall, we evaluate 61 detector/aggregation configurations for each dataset.

#### 4.5. The Baseline Reward Functions

The SPIREL baseline [8] was evaluated using five reward function configurations, which were used primarily to demonstrate SPIREL’s ability to perform well at various cost/performance trade-offs. Another possible reason for the multiple function was the authors’ inability to easily fine-tune their model. This

inability to easily and continuously adapt the performance of the DRL-agent is one of the main novelties of our proposed approach.

To enable a comprehensive and fair comparison, we use the reward functions defined in [8] as our starting point for both of our evaluated datasets. Since these functions were not specifically designed for our evaluated datasets, a high performance by CETRA would further demonstrate its robustness and ability to adapt to changing circumstances. The five reward functions are presented in Table 1. They can generally be divided into two groups— $\{\#1, \#2\}$  and  $\{\#3, \#4, \#5\}$ —based on their underlying rationale.

Table 1: The reward functions used in our experiments are  $C_{2,1} = C_{2,2} = C_2(t)$ . The hyperparameter values for Bahnsen and Wang are  $d_2 = 0.531$  and  $d_2 = 0.8925$ , respectively.

Experiment	TP	TN	FP	FN
1	$C_{2,j}$	$C_{2,j}$	$-C_{2,j}$	$-C_{2,j}$
2	$C_{2,j}$	$C_{2,j}$	$-10C_{2,j}$	$-10C_{2,j}$
3	1	1	$-C_{2,j}$	$-C_{2,j}$
4	10	10	$-C_{2,j}$	$-C_{2,j}$
5	100	100	$-C_{2,j}$	$-C_{2,j}$

**Reward functions #1 & #2.** In these reward functions, both the reward for correct classification and punishment for a mistake are a function of the consumed resources (the two functions differ on the size of the penalty for misclassification). These reward functions are designed to incentivize the DRL-agent to *place greater emphasis on performance compared to cost*. Because the reward for correct classification is also a function of consumed resources, the DRL-agent has an incentive to use all available detectors on samples it concludes it has a high probability of classifying correctly. For difficult-to-classify samples, however, the DRL-agent is faced with a balancing-act where it needs to decide how many resources to “risk” in an attempt to reach a correct classification.

**Reward functions #3 – #5.** In these reward functions, the DRL-agent receives a fixed value for correct classifications, while the cost of an incorrect classification is a function of the computational resources. This reward structure

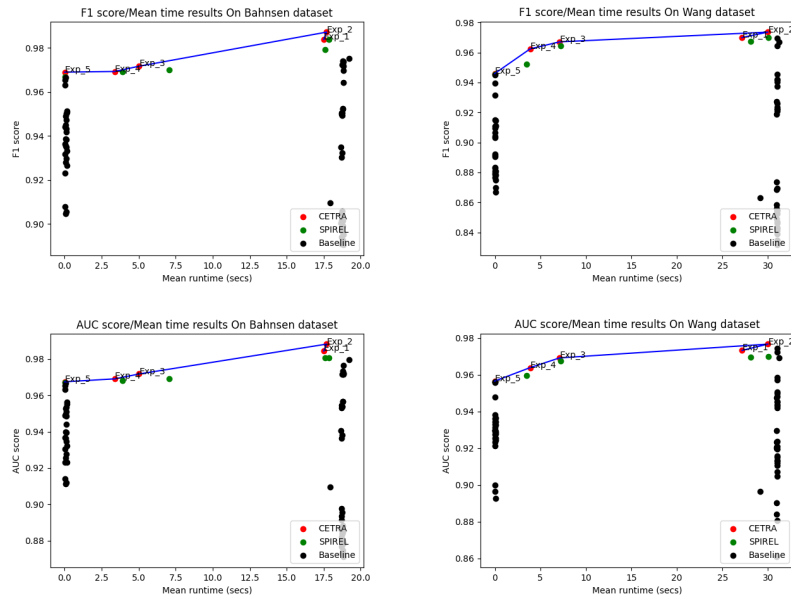


Figure 1: The performance of the baselines on each dataset (F1 and AUC), plotted as a function of the mean time.

incentivizes the DRL-agent to apply as many detectors as it deems necessary to obtain a correct classification, *but not more than that*. The reason is that any detector that does not contribute new information will not increase the reward in case of a correct classification, but will increase the cost in case of a mistake. The DRL-agent must therefore weigh the potential new information a detector can yield against the potential cost of using this detector in case of a mistaken classification.

## 5. EVALUATION AND ANALYSIS

To evaluate CETRA on our two datasets, we first need to create our algorithm’s security policy, i.e., set values for all hyperparameters of our reward function (Equation 8). In Section 5.1, we demonstrate how *we achieve this goal by automatically transferring SPIREL’s security policies* using our novel approach, detailed in Section 3.2.3. Next, in Section 5.2, we demonstrate how CETRA automatically adapts its security policies to meet organizational goals

(e.g., specific recall levels).

### 5.1. Security Policy Transfer

The parameters of SPIREL’s reward function (Equations 4 and 3), while effective, were set empirically. The parameter  $t_1(s)$ , which controls the impact of long running times on the cost, was set to the 95th runtime percentile of each detector. Our goal is to have CETRA build on SPIREL’s policies, but simply copying the latter’s hyperparameters is not likely to yield optimal results. Therefore, we now apply the policy transfer techniques proposed in Section 3.2.3 to set the hyperparameter values in Equations 5 and 6.

As described in Section 3.2.3, our goal is to set a value for the  $d_2$  threshold parameter. Our ‘starting point’ is the function  $C_1(x)$  (Equation 4), where  $d_1 = 1$ ,  $s$  is set to the 95th percentile, and  $t_1(s) = 34$ . Our target function is  $C_2(x)$  (see Equation 6). The likelihood ratio  $\beta_1$  for reference source  $C_1(x)$  is 316.5529. Based on equation 18 and on 19, the empirically chosen solution of  $\beta_2$  is 316.168 for Bahnsen’s dataset, and for Wang’s dataset  $\beta_2$  is chosen to be 316.232, where  $\varepsilon$  is  $10^{-8}$ . Since there is no analytical solution of equation 15, we derived a  $d_2$  with a tolerance of  $10^{-4}$ . We found that for Bahnsen’s dataset that  $d_2 = 0.531$ , and for Wang’s dataset that  $d_2 = 0.8925$ .

Table 2: The top-performing algorithms on the Bahnsen dataset. Note that the complete table is available in Appendix C.11.

Combination	Aggregation	AUC (%)	F1 (%)	Time (sec)	Precision (%)	Recall (%)	Accuracy (%)
<b>CETRA _2</b>	DRL	98.81	98.72	17.69	98.82	98.62	98.62
SPIREL_2	DRL	98.06	98.40	17.847	98.81	97.99	97.76
CETRA _1	DRL	98.43	98.39	17.5	99.47	97.32	98.49
SPIREL_1	DRL	98.05	97.92	17.573	98.86	96.99	97.75
All Detectors Combined	boosting(ADB)	97.94	97.51	19.233	96.81	98.21	97.62
eXpose, PDCNN, XGBoost, FFNN	majority	97.34	97.41	18.7762	97.37	97.45	97.35
All Detectors Combined	majority	97.23	97.37	18.8163	95.91	98.87	97.27
eXpose, PDCNN, CURNN, FFNN	majority	97.16	97.28	18.7783	96.39	98.18	97.19
eXpose, XGBoost, CURNN, FFNN	majority	97.16	97.23	18.7457	97.21	97.25	97.16
PDCNN, XGBoost, CURNN, FFNN	majority	97.14	97.19	18.8135	97.66	96.72	97.13
<b>CETRA _3</b>	DRL	97.09	97.18	5.031	98.72	95.64	96.98
SPIREL_3	DRL	96.91	97.00	7.069	99.03	94.97	97.04
All Detectors Combined	stacking(RF)	97.65	96.97	18.8169	97.80	96.15	98.31
CETRA _4	DRL	96.90	96.93	3.37	98.00	95.86	97.01
SPIREL_4	DRL	96.79	96.91	3.923	96.96	96.85	96.60
CETRA _5	DRL	96.74	96.90	0.002516	96.50	97.30	96.77
SPIREL_5	DRL	96.71	96.68	0.00252	96.85	96.50	96.46

Table 3: The top-performing algorithms on the Wang dataset. Note that the complete table is available in Appendix C.12.

Combination	Aggregation	AUC (%)	F1 (%)	Time (sec)	Precision (%)	Recall (%)	Accuracy (%)
<b>CETRA _2</b>	DRL	97.66	97.36	29.993	97.98	96.74	98.27
SPIREL_2	DRL	96.99	97.01	30.035	98.02	96.00	97.11
CETRA _1	DRL	97.32	97.00	27.1499	99.60	94.40	98.23
All Detectors Combined	stacking(RF)	97.42	96.96	31.041	98.02	95.92	98.32
SPIREL_1	DRL	96.94	96.75	28.074	98.79	94.71	97.09
All Detectors Combined	boosting(ADB)	96.93	96.71	31.247	96.26	97.16	97.11
<b>CETRA _3</b>	DRL	96.91	96.71	7.118	99.34	94.08	97.54
SPIREL_3	DRL	96.73	96.46	7.216	98.92	93.99	97.02
All Detectors Combined	stacking(DT)	97.22	96.44	31.0402	97.53	95.38	98.03
CETRA _4	DRL	96.38	96.24	3.886	99.50	92.99	97.55
SPIREL_4	DRL	95.96	95.21	3.530	99.08	91.34	96.28
CETRA _5	DRL	95.65	94.60	0.0075	95.81	93.39	96.21
SPIREL_5	DRL	95.59	94.55	0.008	95.60	93.50	96.03

We use the approach described above to transfer each of SPIREL’s five policies to our two datasets. The results of our evaluation are presented in Tables 2 & 3 for the Bahnsen and Wang datasets, respectively. Due to space constraints, we only present the top-performing algorithms for each dataset. The results clearly show the following:

**1) CETRA outperforms all the detector combinations.** In both datasets, CETRA outperforms the top-performing detector (CETRA \_2 and \_1) while offering slightly better running times, or achieves slightly lower detection rates (a decrease of 0.5%-1% in AUC) while reducing running time by approximately 75% (CETRA \_3-5).

**2) CETRA outperforms SPIREL in all policy configurations.** In both datasets, all versions of CETRA outperform their ‘origin’ policies, achieving both better detection and running times. This serves as a clear indication that our policy transfer method can effectively and consistently adapt existing policies to new datasets.

CETRA’s clear dominance over SPIREL is important for two reasons. First, it shows that our approach enables ‘zero-shot’ transfer of detection policy, without the need to manually calibrate hyperparameters or run an optimization process. Secondly, the consistent translation demonstrated by our approach—

the preservation of the relative “priorities” of each origin policy—enable us to create a pool of diverse policies that can be used according to circumstance.

Finally, in Figure 1 we plot all evaluated algorithms (detector combinations as well as all SPIREL and CETRA configurations) as a function of their performance and mean runtime per sample. The charts show that CETRA creates a *Pareto frontier*, i.e., for every desired level of performance and/or runtime, CETRA offers the best available solution.

### 5.2. Metric-Driven Policy Adaptations

In the previous section we demonstrated our ability to import and adapt successful policies from one dataset to another. We now evaluate our proposed metric-driven cost function approach (see Section 3.2.2), which enables us to refine policies to meet specific organizational goals (e.g., specific TPR rates).

Table 4: The results of our proposed approach with and without the metric-driven reward function on the Bahnsen dataset. The former is denoted by “Metric”, indicating that it’s the Metric version of CETRA. “Original” indicates that this configuration only uses the density-based transfer.

Combination	AUC (%)	F1 (%)	Time (sec)	Recall (%)
CETRA .1 Metric	98.15	98.10	16.76	98.14
CETRA .1 Original	98.43	98.39	17.5	97.32
CETRA .2 Metric	98.75	98.69	17.12	98.94
CETRA .2 Original	98.81	98.72	17.69	98.62
CETRA .3 Metric	97.04	97.09	5.012	96.21
CETRA .3 Original	97.09	97.18	5.031	95.64
CETRA .4 Metric	96.75	96.94	0.847	97.09
CETRA .4 Original	96.90	96.93	3.37	95.86
CETRA .5 Metric	96.94	96.84	0.0026	97.39
CETRA .5 Original	96.74	96.90	0.0025	97.30

For our evaluation, we chose *Recall as our goal metric*. We define the range 95%-97% as our “acceptable” range, meaning that recall rates above 97% will provide the agent with a bonus score, while values lower than 95% will result in a fine. We chose these values based on CETRA’s performance on the Wang dataset, where all configurations of our approach except CETRA .2 reached recall values below 95%. Because of the very high performance obtained by CETRA for the Bahnsen dataset, we were not able to define a range of values that is beyond the performance of the existing versions of our approach.

Table 5: The results of our proposed approach with and without the metric-driven reward function on the Wang dataset. former is denoted by "Metric", indicating that it's the Metric version of CETRA. "Original" indicates that this configuration only uses the density-based transfer.

Combination	AUC (%)	F1 (%)	Time (sec)	Recall (%)
CETRA _1 Metric	97.73	97.18	30.057	96.41
CETRA _1 Original	97.32	97.00	27.1499	94.40
CETRA _2 Metric	97.61	97.29	30.19	97.02
CETRA _2 Original	97.66	97.36	29.993	96.74
CETRA _3 Metric	96.84	96.52	3.155	95.54
CETRA _3 Original	96.91	96.71	7.118	94.08
CETRA _4 Metric	96.44	95.92	1.393	95.83
CETRA _4 Original	96.38	96.24	3.886	92.99
CETRA _5 Metric	95.50	94.56	0.002758	95.21
CETRA _5 Original	95.65	94.60	0.0075	93.39

The results of our initial experiments (named 'Original') and the metric-based ones (named 'Metric') for the Bahnsen and Wang datasets (named 'After') are presented in Tables 4 and 5, respectively. We focus first on the Wang dataset, where CETRA performance with respect to the recall metric was not in the specified range in 4 out of 5 configurations. The new results clearly show that our metric-driven approach achieved its goals: the recall values of all CETRA configurations now fall within the specified range. Interestingly, the added requirement we placed on our DRL-agent had the effect of providing an additional boost to its performance: both in terms of F1-score and AUC, our approach was able to achieve higher performance compared to the baselines. Additionally, for two configurations – #3 and #4 – our metric-driven approach yielded significantly shortened running times (in the remaining three configurations, the differences were insignificant).

While the performance of CETRA was already within the predefined recall rang for the Bahnsen dataset, an analysis of the results showed that our metric-driven approach improved the average running time of our approach in three configurations, slightly extended it in one, and left the remaining configuration unchanged. The reduction in running time is particularly notable for configuration #4, where the average running time dropped from 3.37s to 0.847s, without any impact on the F1 score.

We attribute this improvement in performance and/or running time to the



added incentive our agent now has to exceed the threshold of 97% recall. Once our approach crosses this line, it receives a “bonus” reward to its overall performance. The DRL-agent therefore has the incentive to *slightly exceed the 97% threshold*, and then direct its attention to improving the overall performance, so it can maximize its bonus. A clear example of this is the Bahnsen dataset: the F1 rates of CETRA \_2 dropped from 98.72% to 98.69%, but its recall rates rose from 98.62% to 98.94%.

In conclusion, our metric-driven goals are an effective way to create a more nuanced security policy without the need for complex configuration and/or hyper-parameter search. Organizations are able to first quantify the actual cost of deploying various detectors, and then add an additional constraints to specify the performance metrics they would like to achieve. The DRL-agent then refined its policy to best meet those requirements.

## 6. ROBUSTNESS EVALUATION

DRL-based solutions have been shown to be vulnerable to adversarial machine learning (AML) attacks [40, 41, 42, 43, 44, 45, 46]. We hypothesize that CETRA’s hierarchical structure, which dynamically selects additional detectors based on the scores of previous ones, would make AML attacks more difficult to execute. To test our hypothesis, we evaluate both black-box and white-box attacks. Additionally, because of CETRA’s focus on efficiency, we evaluate an adversarial attack that seeks to cause larger resource usage.

Note that in all our experiments, *we operate under the strong assumption that the attacker can modify each URL to achieve any desired score from individual detectors*. Under this (highly beneficial to the attacker) assumption, the attack focuses solely on manipulating the DRL agent’s ‘decision process’. For this reason, we expect adversarial attacks to be even less effective in a fully realistic setup.

### 6.1. Evasion – White-box gradient based attack

We implemented two variants of an adaptive attack, using two gradient-based white-box attacks: PGD [47] and FSGM [48]. The attack is applied to CETRA as follows: for each attacked sample, we retrieve the full (pre-attack) trajectory of states  $\{s_t\}_{t=1}^T$  chosen by the DRL agent, where  $s_t \in S^n$ ,  $S = \{-1\} \cup [0, 1]$  and  $n$  is the number of base detectors. Then, we generate the perturbed trajectory  $\{\hat{s}_t\}_{t=1}^{\hat{T}}$ : in the first timestamp  $t = 1$ , we define  $\hat{s}_1 = s_1$ . Then, for each timestamp  $t \geq 2$ ,  $\hat{w}_t$  is the result of the targeted PGD/FSGM algorithms on  $\hat{s}_{t-1}$ , such that for  $p = \infty$ ,  $\sum_{t=1}^{\hat{T}-1} \|\hat{s}_t - \hat{w}_t\|_p \leq \varepsilon$ . Then,  $\hat{s}_t$  is the state reached by following the trained policy  $\pi$  on  $\hat{w}_t$  and action  $\hat{a}_t$  (i.e., the result of following the perturbed trajectory).

Since the number of steps cannot be larger than the number of detectors  $\hat{T} - 1 \leq n$ , we choose a sequence  $\{\varepsilon_t\}_{t=1}^n$ , such that at each timestamp  $t$ , we craft a perturbation  $\hat{w}_t$  in  $L_p$  under the current budget  $\varepsilon_t$ . From that, we can derive the following:

$$\sum_{t=1}^{\hat{T}-1} \|\hat{s}_t - \hat{w}_t\|_p \leq \sum_{t=1}^n \|\hat{s}_t - \hat{w}_t\|_p \leq \sum_{t=1}^n \varepsilon_t \leq \varepsilon \quad (20)$$

where  $\sum_{t=1}^n \varepsilon_t \leq \varepsilon$  is a necessary condition to meet the requirements of an  $L_p$  attack under the current budget  $\varepsilon$ .

We evaluated three attack scenarios: 1) Utilize all the budget at once, defined as:  $\varepsilon_t = \varepsilon \mathbf{I}_{\{k\}}(t)$ , where  $k = 1, 2, \dots, n$  and  $\mathbf{I}$  is an indicator function; 2) Utilize the budget uniformly over the trajectory, defined as:  $\varepsilon_t = \frac{\varepsilon}{n}$ ; 3) Utilizes the budget in a geometric decay sequence, defined as:  $\varepsilon_t = \varepsilon q^t$ , where  $q \leq \frac{1}{2}$ . We use the same two datasets and CETRA 2 and 3 for our evaluation. We perform the attacks over the  $L_\infty$  norm, and use epsilon values (i.e., perturbation size budget) of 0.1, 0.25, 0.5 for PGD and 0.5 for FSGM. The number of phishing samples chosen (randomly) for perturbation was 10,000, with results averaged over three randomly-initiated experiments.

Our results, presented in Figure 2 (a), show that the adversarial attack evade

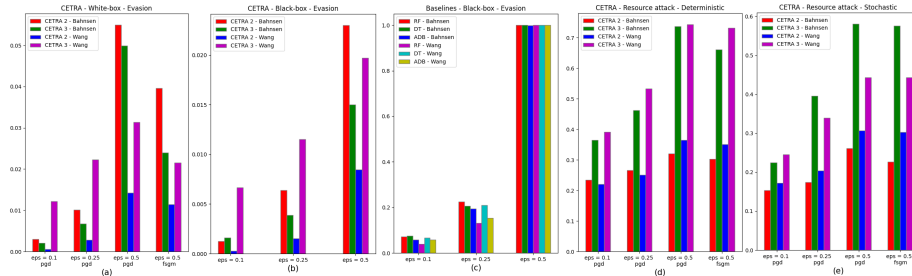


Figure 2: The results of evasion and resource-consumption attacks on CETRA and the baseline models. We present results for white-box evasion attacks (a), black-box evasion attacks (b-c), and resource consumption attacks (d-e). We present results for CETRA configurations 2 and 3. please note the different scale of the y-axis of the graphs.

detection by CETRA in only 5.5% of the attempts, and under a large epsilon (budget) of 0.5. The attack fared worse for lower budgets. Additionally, to evade detection, the attack needed to craft a perturbed state in which on average two detector scores are changed, and the magnitude of change (compared with the original state) was 0.07, 0.17 and 0.32 for epsilon 0.1, 0.25 and 0.5, respectively.

These results indicate that CETRA is highly robust to AML evasion attacks, even without any enhancements.

## 6.2. Evasion – Black-box attack

Gradient-based adversarial attacks (e.g., PGD and FSGM) cannot be applied to our baseline ensemble methods, as they don’t use gradients. Therefore, we use the following attack procedure to evaluate their and CETRA’s robustness: Instead of perturbing individual states, we randomly perturb the input vector  $s$  in  $L_p$  at each time stamp  $t$  using budget  $\varepsilon$ . We do so by adding or subtracting  $\varepsilon$  from each feature in the vector. In essence, we utilize all the budget at once (i.e.,  $\varepsilon_t = \varepsilon \mathbf{I}_{\{k\}}(t)$ , where  $k = 1, 2, \dots, n$  and  $\mathbf{I}$  is an indicator function). For the baselines, which are not sequence-based algorithms, we create  $\hat{s}$  by randomly perturbing the input vector  $s$  in  $L_p$  by adding or subtracting  $\varepsilon$  to each feature in the vector.

We use the same experimental setup as Section 6.1. Our results are presented in Figure 2 (b). For CETRA the adversarial attack managed to evade detection

in only 2.3% of the attempts and under a large epsilon value of 0.5—worse results than the white-box attack. To evade detection by CETRA, the attack needed to craft a perturbed state in which on average two detector scores are changed, and the magnitude of change (compared with the original state) is 0.13, 0.19 and 0.41 for epsilon 0.1, 0.25 and 0.5, respectively. As for the baselines (Figure 2 (c)), almost 20% of the attack attempts managed to evade detection for  $\epsilon$  value of 0.25, and 100% under  $\epsilon = 0.5$ .

### 6.3. Resource utilization attack

CETRA main objective is to reduce the computational cost of detection. We now consider adversarial attacks designed to prolong its running time by tricking it into calling additional detectors. We modified the attack presented in section 6.1 so that from all trajectories that result in the same class, we choose the one where the largest number of detectors were called or with a larger total time than before. We use the same setup as in the section 6.1, and evaluate two versions of our approach: a *deterministic case*, where the DRL agent’s actions are deterministic, and a *stochastic case* where the probability of choosing an action is proportional to its score.

The results of the attack for the deterministic case are presented in Figure 2 (d). For both datasets, the attack succeeded in increasing CETRA \_2’s resource consumption by 33.5% for  $\epsilon = 0.5$ , for PGD and FSGM. For CETRA \_3, the attack was more effective, with a 73.5% increase for  $\epsilon = 0.5$ .

The magnitude of sample change needed for a successful attack is 0.08, 0.11 and 0.19 for epsilon 0.1, 0.25 and 0.5, respectively.

The reason for this difference in robustness is CETRA \_2’s tendency to deploy more detectors due to its focus on detection, whereas CETRA \_3 gives greater weight to efficiency and tends to call fewer detectors.

The results of the attack for the *stochastic case* are presented in Figure 2 (e). Compared to the previous success rate of the deterministic case, the success rate on both datasets for CETRA \_2 reduced by 7.5% for  $\epsilon = 0.5$ , either by using PGD or FSGM. As for CETRA \_3, the attack success rate was reduced even

more to 19.5% on average for  $\varepsilon = 0.5$ . The attack needed to craft a perturbed state in which on average two detector scores are changed, and the magnitude of change (compared with the original state) is now 0.12, 0.23 and 0.31 for epsilon 0.1, 0.25 and 0.5, respectively.

The stochastic policy has a minor effect on performance/runtime. For the Bahnsen dataset, CETRA \_2's F1 score was reduced from 98.72% to 98.39%, while CETRA \_3's was reduced from 97.18% to 96.98%. Similar results were obtained for the Wang dataset. The differences in the running time with and without the stochastic policy were negligible—0.114 milliseconds on average.

## 7. CONCLUSIONS

Utilizing DRL-based solutions in the security domain is challenging both because of the difficulty to calibrate the reward function for new datasets, and because of the need to meet multiple criteria that are possibly not integrated into the reward function. In this study we address both challenges: first, we propose a method of intelligently importing effective security policies from other datasets, thus removing the need for time-consuming optimization. Secondly, we present a method for refining existing policies so that they take into account any additional metrics (and value ranges) desirable to the organization. Evaluation on two real-world datasets shows that our approach is both flexible and effective.

## References

- [1] Y. Ren, L. Zhang, P. N. Suganthan, Ensemble classification and regression—recent developments, applications and future directions, *IEEE Computational intelligence magazine* 11 (2016) 41–53.
- [2] N. Dvornik, C. Schmid, J. Mairal, Diversity with cooperation: Ensemble methods for few-shot classification, in: *Proceedings of the IEEE/CVF international conference on computer vision*, 2019, pp. 3723–3731.

- [3] K. Belitz, P. Stackelberg, Evaluation of six methods for correcting bias in estimates from ensemble tree machine learning regression models, *Environmental Modelling & Software* 139 (2021) 105006.
- [4] S. Gupta, A. Gupta, Dealing with noise problem in machine learning datasets: A systematic review, *Procedia Computer Science* 161 (2019) 466–474.
- [5] J. Brajard, A. Carrassi, M. Bocquet, L. Bertino, Combining data assimilation and machine learning to emulate a dynamical model from sparse and noisy observations: A case study with the lorenz 96 model, *Journal of Computational Science* 44 (2020) 101171.
- [6] D. Li, Q. Li, Adversarial deep ensemble: Evasion attacks and defenses for malware detection, *IEEE Transactions on Information Forensics and Security* 15 (2020) 3886–3900.
- [7] H. Yang, J. Zhang, H. Dong, N. Inkawhich, A. Gardner, A. Touchet, W. Wilkes, H. Berry, H. Li, Dverge: diversifying vulnerabilities for enhanced robust generation of ensembles, *Advances in Neural Information Processing Systems* 33 (2020) 5505–5515.
- [8] Y. Birman, S. Hindi, G. Katz, A. Shabtai, Cost-effective ensemble models selection using deep reinforcement learning, *Information Fusion* 77 (2022) 133–148.
- [9] G. Xiang, J. Hong, C. P. Rose, L. Cranor, Cantina+ a feature-rich machine learning framework for detecting phishing web sites, *ACM Transactions on Information and System Security (TISSEC)* 14 (2011) 1–28.
- [10] M. H. S. Horng, P. Fan, M. Khan, R. Run, J. L. R. Chen, An efficient phishing webpage detector expertsystems with applications, *An International Journal* 38 (2011).
- [11] D. Zhang, Z. Yan, H. Jiang, T. Kim, A domain-feature enhanced classification model for the detection of chinese phishing e-business websites, *Information & Management* 51 (2014) 845–853.

- [12] R. M. Mohammad, F. Thabtah, L. McCluskey, Predicting phishing websites based on self-structuring neural network, *Neural Computing and Applications* 25 (2014) 443–458.
- [13] R. Verma, K. Dyer, On the character of phishing urls: Accurate and robust statistical learning classifiers, in: *Proceedings of the 5th ACM Conference on Data and Application Security and Privacy*, 2015, pp. 111–122.
- [14] M. Moghimi, A. Y. Varjani, New rule-based phishing detection method, *Expert systems with applications* 53 (2016) 231–242.
- [15] W. Zhang, Q. Jiang, L. Chen, C. Li, Two-stage elm for phishing web pages detection using hybrid features, *World Wide Web* 20 (2017) 797–813.
- [16] A. C. Bahnsen, E. C. Bohorquez, S. Villegas, J. Vargas, F. A. González, Classifying phishing urls using recurrent neural networks, in: *2017 APWG symposium on electronic crime research (eCrime)*, IEEE, 2017, pp. 1–8.
- [17] J. Saxe, K. Berlin, expose: A character-level convolutional neural network with embeddings for detecting malicious urls, file paths and registry keys, *arXiv preprint arXiv:1702.08568* (2017).
- [18] H. Le, Q. Pham, D. Sahoo, S. C. Hoi, Urlnet: Learning a url representation with deep learning for malicious url detection, *arXiv preprint arXiv:1802.03162* (2018).
- [19] W. Wang, F. Zhang, X. Luo, S. Zhang, Pdcnn: Precise phishing detection with recurrent convolutional neural networks, *Security and Communication Networks* 2019 (2019).
- [20] G. Kalweit, J. Boedecker, Uncertainty-driven imagination for continuous deep reinforcement learning, in: *Conference on Robot Learning*, 2017, pp. 195–206.
- [21] H. Van Hasselt, A. Guez, D. Silver, Deep reinforcement learning with double q-learning, in: *Proceedings of the AAAI Conference on Artificial Intelligence*, volume 30, 2016.

- [22] V. Mnih, K. Kavukcuoglu, D. Silver, A. A. Rusu, J. Veness, M. G. Bellemare, A. Graves, M. Riedmiller, A. K. Fidjeland, G. Ostrovski, et al., Human-level control through deep reinforcement learning, *nature* 518 (2015) 529–533.
- [23] C. Colas, O. Sigaud, P.-Y. Oudeyer, Gep-pg: Decoupling exploration and exploitation in deep reinforcement learning algorithms, in: *International conference on machine learning*, PMLR, 2018, pp. 1039–1048.
- [24] K. Zhou, Y. Qiao, T. Xiang, Deep reinforcement learning for unsupervised video summarization with diversity-representativeness reward, in: *Proceedings of the AAAI Conference on Artificial Intelligence*, volume 32, 2018.
- [25] J. Feng, M. Huang, L. Zhao, Y. Yang, X. Zhu, Reinforcement learning for relation classification from noisy data, in: *Proceedings of the aaai conference on artificial intelligence*, volume 32, 2018.
- [26] J. J. Blount, D. R. Tauritz, S. A. Mulder, Adaptive rule-based malware detection employing learning classifier systems: a proof of concept, in: *2011 IEEE 35th Annual Computer Software and Applications Conference Workshops*, IEEE, 2011, pp. 110–115.
- [27] S. Smadi, N. Aslam, L. Zhang, Detection of online phishing email using dynamic evolving neural network based on reinforcement learning, *Decision Support Systems* 107 (2018) 88–102.
- [28] J. Fu, K. Luo, S. Levine, Learning robust rewards with adversarial inverse reinforcement learning, *arXiv preprint arXiv:1710.11248* (2017).
- [29] H. S. Anderson, A. Kharkar, B. Filar, D. Evans, P. Roth, Learning to evade static pe machine learning malware models via reinforcement learning, *arXiv preprint arXiv:1801.08917* (2018).



- [30] K. Mo, W. Tang, J. Li, X. Yuan, Attacking deep reinforcement learning with decoupled adversarial policy, *IEEE Transactions on Dependable and Secure Computing* (2022).
- [31] F. Raiber, O. Kurland, Kullback-leibler divergence revisited, in: *Proceedings of the ACM SIGIR International Conference on Theory of Information Retrieval*, 2017, pp. 117–124.
- [32] S. Tabibian, A. Akbari, B. Nasersharif, Speech enhancement using a wavelet thresholding method based on symmetric kullback-leibler divergence, *Signal Processing* 106 (2015) 184–197.
- [33] A. K. Jain, B. B. Gupta, A machine learning based approach for phishing detection using hyperlinks information, *Journal of Ambient Intelligence and Humanized Computing* 10 (2019) 2015–2028.
- [34] T. Chen, T. He, M. Benesty, V. Khotilovich, Y. Tang, Xgboost: extreme gradient boosting, *R package version 0.4-2* (2015) 1–4.
- [35] G. Brockman, V. Cheung, L. Pettersson, J. Schneider, J. Schulman, J. Tang, W. Zaremba, Openai gym, *arXiv preprint arXiv:1606.01540* (2016).
- [36] L.-J. Lin, Self-improving reactive agents based on reinforcement learning, planning and teaching, *Machine learning* 8 (1992) 293–321.
- [37] A. Nandy, M. Biswas, Reinforcement learning with keras, tensorflow, and chainerrl, in: *Reinforcement Learning*, Springer, 2018, pp. 129–153.
- [38] T. Tieleman, G. Hinton, Lecture 6.5-rmsprop: Divide the gradient by a running average of its recent magnitude, *COURSERA: Neural networks for machine learning* 4 (2012) 26–31.
- [39] D. Zhang, J. Wang, X. Zhao, Estimating the uncertainty of average fl scores, in: *Proceedings of the 2015 International conference on the theory of information retrieval*, 2015, pp. 317–320.

- [40] I. Rosenberg, A. Shabtai, Y. Elovici, L. Rokach, Adversarial learning in the cyber security domain (2020).
- [41] S. Huang, N. Papernot, I. Goodfellow, Y. Duan, P. Abbeel, Adversarial attacks on neural network policies, arXiv preprint arXiv:1702.02284 (2017).
- [42] J. Kos, D. Song, Delving into adversarial attacks on deep policies, arXiv preprint arXiv:1705.06452 (2017).
- [43] Y.-C. Lin, Z.-W. Hong, Y.-H. Liao, M.-L. Shih, M.-Y. Liu, M. Sun, Tactics of adversarial attack on deep reinforcement learning agents, arXiv preprint arXiv:1703.06748 (2017).
- [44] J. Sun, T. Zhang, X. Xie, L. Ma, Y. Zheng, K. Chen, Y. Liu, Stealthy and efficient adversarial attacks against deep reinforcement learning, in: Proceedings of the AAAI Conference on Artificial Intelligence, volume 34, 2020, pp. 5883–5891.
- [45] I. Ilahi, M. Usama, J. Qadir, M. U. Janjua, A. Al-Fuqaha, D. T. Huang, D. Niyato, Challenges and countermeasures for adversarial attacks on deep reinforcement learning, IEEE Transactions on Artificial Intelligence (2021).
- [46] E. Tretschk, S. J. Oh, M. Fritz, Sequential attacks on agents for long-term adversarial goals, arXiv preprint arXiv:1805.12487 (2018).
- [47] A. Madry, A. Makelov, L. Schmidt, D. Tsipras, A. Vladu, Towards deep learning models resistant to adversarial attacks, arXiv preprint arXiv:1706.06083 (2017).
- [48] I. J. Goodfellow, J. Shlens, C. Szegedy, Explaining and harnessing adversarial examples, arXiv preprint arXiv:1412.6572 (2014).
- [49] D. Markechová, Kullback-leibler divergence and mutual information of experiments in the fuzzy case, Axioms 6 (2017) 5.
- [50] F. Baccelli, P. Brémaud, Palm probabilities and stationary queues, volume 41, Springer Science & Business Media, 2012.

## Appendix A. Detector Performance Analysis

For an ensemble to perform well, the detectors need to have *meaningful differences in performance*, meaning that one detector is capable of correctly classifying samples another detector could not. Moreover, it is important to ensure that no detector “dominates” another, i.e., achieves an equal or more accurate classification for every sample. Our analysis in this section demonstrates that these two conditions are met. Throughout this section, we use standard practices and evaluation metrics. Given that all our detectors output classifications in the range of  $[0, 1]$ , we use the following setting to determine the classification of each sample:

$$p_i = \begin{cases} \textit{benign} & , \textit{prediction} \leq 0.5 \\ \textit{phishing} & , \textit{otherwise} \end{cases} \quad (\text{A.1})$$

Table A.6: The performance of the individual detectors on the Bahnsen dataset.

Detector	AUC (%)	F1 (%)	Time (sec)	Precision (%)	Recall (%)	Accuracy (%)
CURNN	96.42	96.31	0.0400	95.71	96.91	96.40
eXpose	96.58	96.53	0.0025	94.31	98.75	96.51
XGBoost	92.58	92.30	0.0379	95.51	89.09	92.69
PDRCNN	96.76	96.66	0.0609	96.16	97.17	96.75
FFNN	90.96	90.96	17.9453	87.97	93.95	90.86

Table A.7: The performance of the individual detectors on the Wang dataset

Detector	AUC (%)	F1 (%)	Time (sec)	Precision (%)	Recall (%)	Accuracy (%)
CURNN	95.62	94.52	0.01831	95.40	93.63	96.23
eXpose	95.56	93.94	0.0024	92.94	94.95	95.75
XGBoost	92.54	90.65	0.0377	92.23	89.06	93.61
PDRCNN	94.78	93.17	0.0390	93.14	93.20	95.26
FFNN	89.65	86.29	29.1686	85.24	87.34	90.36

The performance of our detectors for the two datasets described in Section 4.1 is presented in Tables A.6 & A.7. It is clear that all detectors have high yet diverse rates of precision and recall, a fact that satisfies our first requirement. Moreover, it is clear that there is large variance in the detectors’ average

running time per sample, a fact that makes the selection of a subset of them potentially very cost-effective.

Next, we analyze the performance of the detectors to determine whether the performance of any of them is dominated by another. Our analysis is performed as follows: for each detector, we only consider the samples that were *classified incorrectly*. Next, for these samples, we analyze the performance of all other detectors to determine for each of them whether it is able to correctly classify at least some of them. If that is the case, we can conclude that the latter detectors are not being dominated by the former. The results of this analysis are presented in Tables A.8 & A.9. It is clear that no detector dominates another, and that the ability of one detector to compensate for the failings of another is often high. It should also be noted that FFNN, the detector whose performance was a little lower than those of the other detectors (see Tables A.6 & A.7), has the best average performance in this analysis.

To conclude, in this section we were able to show that not only do our detectors have high performance rates in their own right, combining them in an ensemble has the potential to yield non-trivial improvement in performance. In the following section we describe how CETRA can be used to improve upon the performance of the standard ensemble.

Table A.8: Percentage of URLs mis-classified by one detector (row) and correctly classified by another (column) – Bahnsen dataset.

Method	CURNN (%)	eXpose (%)	XGBoost (%)	PDRCNN (%)	FFNN (%)
CURNN	-	41.94	62.6	48.41	69.81
eXpose	45.36	-	71.34	45.76	66.45
XGBoost	81.38	84.83	-	84.86	81.03
PDRCNN	43.36	36.71	66.61	-	71.11
FFNN	87.35	85.06	84.04	88.97	-

## Appendix B. Dataset transferability experiment

The goal of this set of experiments is to evaluate the robustness and transferability of the policies generated by our proposed approach. To this end, we train our full model (using the density-based transfer learning + metric-driven cost

Table A.9: Percentage of URLs mis-classified by one detector (row) and correctly classified by another (column) – Wang dataset.

Method	CURNN (%)	eXpose (%)	XGBoost (%)	PDRCNN (%)	FFNN (%)
CURNN	-	41.56	45.46	36.7	84.5
eXpose	49.93	-	57.84	45.53	85.57
XGBoost	65.20	68.60	-	63.27	86.37
PDRCNN	48.76	48.53	53.39	-	85.39
FFNN	93.09	92.59	90.48	91.96	-

function) on the training set of one of our datasets, then apply it to the test set of another.

The results of our evaluation are presented in Table B.10. The results clearly show that our generated policies perform very well when applied to different datasets with similar characteristics. It should also be pointed out that our various reward function configurations maintain the same relative ranking in the performance/runtime trade-offs, further demonstrating the robustness and stability of our approach.

Table B.10: CETRA’s performance in a transfer-learning setting. We train our approach on one dataset, then apply it to the other.

Train set	Test set	Combination	AUC (%)	F1 (%)	Time (sec)	Precision (%)	Recall (%)	Accuracy (%)
Wang	Bahnsen	<b>CETRA _2</b>	99.08	99.04	18.57	99.27	98.82	99.10
Wang	Bahnsen	CETRA _1	98.76	98.71	17.32	98.87	98.55	98.77
Wang	Bahnsen	<b>CETRA _3</b>	98.51	98.46	5.141	99.03	97.89	98.53
Wang	Bahnsen	CETRA _4	98.00	97.71	2.74	96.59	98.86	97.91
Wang	Bahnsen	CETRA _5	96.90	96.80	0.0057	95.55	98.09	96.86
Bahnsen	Wang	<b>CETRA _2</b>	96.88	96.60	27.641	99.20	94.14	97.82
Bahnsen	Wang	CETRA _1	96.72	95.61	27.441	95.15	96.07	96.92
Bahnsen	Wang	<b>CETRA _3</b>	95.30	95.03	7.666	99.82	90.67	96.95
Bahnsen	Wang	CETRA _4	94.89	94.18	2.97	97.24	91.30	95.84
Bahnsen	Wang	CETRA _5	94.40	93.89	0.00238	98.90	89.37	95.95

### Appendix C. Full Results

The full results of our evaluation are presented in Tables C.11 & C.12 for the Bahnsen and Wang datasets, respectively.

Table C.11: Full description of methods' results on Bahnsen's dataset (ordered based on the F1 score).

Combination	Aggregation	AUC (%)	F1 (%)	Time (sec)	Precision (%)	Recall (%)	Accuracy (%)
<b>CETRA _2</b>	DRL	98.81	98.72	17.69	98.82	98.62	98.62
SPIREL_2	DRL	98.06	98.40	17.847	98.81	97.99	97.76
CETRA _1	DRL	98.43	98.39	17.5	99.47	97.32	98.49
SPIREL_1	DRL	98.05	97.92	17.573	98.86	96.99	97.75
All Detectors Combined	boosting(ADB)	97.94	97.51	19.233	96.81	98.21	97.62
eXpose, PDRCNN, XGBoost, FFNN	majority	97.34	97.41	18.7762	97.37	97.45	97.35
All Detectors Combined	majority	97.23	97.37	18.8163	95.91	98.87	97.27
eXpose, PDRCNN, CURNN, FFNN	majority	97.16	97.28	18.7783	96.39	98.18	97.19
eXpose, XGBoost, CURNN, FFNN	majority	97.16	97.23	18.7457	97.21	97.25	97.16
PDRCNN, XGBoost, CURNN, FFNN	majority	97.14	97.19	18.8135	97.66	96.72	97.13
<b>CETRA _3</b>	DRL	97.09	97.18	5.031	98.72	95.64	96.98
SPIREL_3	DRL	96.91	97.00	7.069	99.03	94.97	97.04
All Detectors Combined	stacking(RF)	97.65	96.97	18.8169	97.80	96.15	98.31
CETRA _4	DRL	96.90	96.93	3.37	98.00	95.86	97.01
SPIREL_4	DRL	96.79	96.91	3.923	96.96	96.85	96.60
CETRA _5	DRL	96.74	96.90	0.002516	96.50	97.30	96.77
SPIREL_5	DRL	96.71	96.68	0.00252	96.85	96.50	96.46
All Detectors Combined	stacking(DT)	97.17	96.42	18.8165	97.63	95.24	98.02
PDRCNN, CURNN, FFNN	majority	95.66	95.24	18.7730	94.97	95.51	95.67
PDRCNN, XGBoost, FFNN	majority	95.67	95.21	18.7745	95.44	94.98	95.66
eXpose, PDRCNN, XGBoost, CURNN	majority	95.61	95.13	0.1510	95.77	94.48	95.59
PDRCNN, XGBoost, CURNN	majority	95.52	95.06	0.1485	95.34	94.77	95.51
eXpose, XGBoost, FFNN	majority	95.44	95.05	18.7070	94.58	95.51	95.45
eXpose, PDRCNN, FFNN	majority	95.37	95.03	18.7388	94.06	95.99	95.39
eXpose, PDRCNN, XGBoost	majority	95.34	95.02	0.1121	94.53	95.51	95.42
eXpose, CURNN, FFNN	majority	95.32	94.98	18.7080	93.94	96.01	95.34
XGBoost, CURNN, FFNN	majority	95.38	94.93	18.7443	95.13	94.73	95.37
eXpose, XGBoost, CURNN	majority	95.28	94.89	0.0802	94.49	95.29	95.29
eXpose, PDRCNN, CURNN	majority	95.10	94.74	0.1130	94.00	95.48	95.12
eXpose, PDRCNN	majority	94.97	94.50	0.0732	95.20	93.79	94.95
eXpose, CURNN	majority	94.88	94.41	0.0424	95.13	93.68	94.86
PDRCNN, CURNN	majority	94.85	94.32	0.1107	96.03	92.60	94.80
PDRCNN, CURNN	or	94.40	94.18	0.1104	92.52	95.83	94.44
eXpose, PDRCNN	or	93.97	93.87	0.0731	91.50	96.23	94.03
PDRCNN, XGBoost	or	93.94	93.83	0.1085	91.57	96.08	94.00
eXpose, CURNN	or	93.68	93.64	0.0423	91.00	96.27	93.75
XGBoost, CURNN	or	93.64	93.55	0.0777	91.26	95.83	93.70
eXpose, PDRCNN, CURNN	or	93.47	93.50	0.1129	90.56	96.43	93.55
eXpose, FFNN	majority	94.04	93.48	18.6682	96.29	90.66	93.97
PDRCNN, XGBoost, CURNN	or	93.23	93.31	0.1483	90.13	96.49	93.32
PDRCNN, FFNN	majority	93.82	93.23	18.7363	97.17	89.28	93.72
eXpose, XGBoost	or	93.04	93.17	0.0404	89.73	96.61	93.13
CURNN, FFNN	majority	93.64	93.04	18.7053	96.86	89.22	93.54
eXpose, PDRCNN, XGBoost	or	92.77	92.98	0.1110	89.24	96.71	92.87
eXpose, XGBoost, CURNN	or	92.54	92.80	0.0802	88.88	96.72	92.65
eXpose, PDRCNN, XGBoost, CURNN	or	92.32	92.65	0.1508	88.52	96.77	92.44
eXpose, XGBoost	majority	91.42	90.77	0.0404	96.77	84.77	91.27
PDRCNN, FFNN	or	89.56	90.57	18.7362	84.54	96.60	89.74
PDRCNN, XGBoost	majority	91.21	90.56	0.1087	97.34	83.78	91.03
XGBoost, CURNN	majority	91.13	90.47	0.0779	96.98	83.96	90.96
CURNN, FFNN	or	89.36	90.47	18.7054	84.28	96.65	89.54
XGBoost, FFNN	or	89.14	90.16	18.7035	84.39	95.93	89.32
PDRCNN, CURNN, FFNN	or	88.82	90.14	18.7760	83.45	96.82	89.03
eXpose, FFNN	or	88.65	90.02	18.6681	83.22	96.81	88.86
PDRCNN, XGBoost, FFNN	or	88.49	89.92	18.7741	82.98	96.85	88.70
eXpose, PDRCNN, FFNN	or	88.40	89.86	18.7387	82.86	96.86	88.62
XGBoost, CURNN, FFNN	or	88.38	89.84	18.7433	82.84	96.84	88.60
eXpose, CURNN, FFNN	or	88.19	89.72	18.7079	82.57	96.86	88.41
eXpose, PDRCNN, CURNN, FFNN	or	87.99	89.60	18.7785	82.30	96.89	88.21
PDRCNN, XGBoost, CURNN, FFNN	or	87.86	89.52	18.8139	82.12	96.91	88.09
eXpose, XGBoost, FFNN	or	87.69	89.41	18.7060	81.89	96.92	87.93
eXpose, PDRCNN, XGBoost, FFNN	or	87.46	89.26	18.7766	81.58	96.94	87.70
eXpose, XGBoost, CURNN, FFNN	or	87.30	89.16	18.7458	81.37	96.94	87.54
XGBoost, FFNN	majority	89.76	89.07	18.7034	96.75	81.38	89.56
All Detectors Combined	or	87.11	89.04	18.8164	81.13	96.95	87.36

Table C.12: Full description of methods' results on Wang's dataset (ordered by F1 score).

Combination	Aggregation	AUC (%)	F1 (%)	Time (sec)	Precision (%)	Recall (%)	Accuracy (%)
<b>CETRA .2</b>	DRL	97.66	97.36	29.993	97.98	96.74	98.27
SPiREL.2	DRL	96.99	97.01	30.035	98.02	96.00	97.11
CETRA .1	DRL	97.32	97.00	27.1499	99.60	94.40	98.23
All Detectors Combined	stacking(RF)	97.42	96.96	31.041	98.02	95.92	98.32
SPiREL.1	DRL	96.94	96.75	28.074	98.79	94.71	97.09
All Detectors Combined	boosting(ADB)	96.93	96.71	31.247	96.26	97.16	97.11
<b>CETRA .3</b>	DRL	96.91	96.71	7.118	99.34	94.08	97.54
SPiREL.3	DRL	96.73	96.46	7.216	98.92	93.99	97.02
All Detectors Combined	stacking(DT)	97.22	96.44	31.0402	97.53	95.38	98.03
CETRA .4	DRL	96.38	96.24	3.886	99.50	92.99	97.55
SPiREL.4	DRL	95.96	95.21	3.530	99.08	91.34	96.28
CETRA .5	DRL	95.65	94.60	0.0075	95.81	93.39	96.21
SPiREL.5	DRL	95.59	94.55	0.008	95.60	93.50	96.03
eXpose, XGBoost, CURNN, FFNN	majority	94.97	94.22	30.99175	98.13	90.62	96.88
eXpose, PDRCNN, CURNN, FFNN	majority	95.06	94.15	30.9965	97.48	91.04	96.82
eXpose, PDRCNN, XGBoost, FFNN	majority	94.83	94.02	31.0143	97.91	90.42	96.76
PDRCNN, XGBoost, CURNN, FFNN	majority	94.53	93.75	31.0317	98.13	89.74	96.63
eXpose, CURNN, FFNN	majority	94.75	92.74	30.9561	93.43	92.04	95.61
XGBoost, CURNN, FFNN	majority	94.37	92.59	30.9892	94.19	90.98	95.54
PDRCNN, CURNN, FFNN	majority	94.29	92.36	30.9948	93.73	90.99	95.41
eXpose, PDRCNN, FFNN	majority	94.49	92.24	30.9789	92.62	91.85	95.33
PDRCNN, XGBoost, FFNN	majority	94.18	92.20	31.0133	93.53	90.86	95.32
eXpose, XGBoost, FFNN	majority	95.85	92.08	30.9737	92.24	91.92	94.51
eXpose, FFNN	majority	89.04	91.90	30.9368	96.20	87.60	92.90
eXpose, XGBoost, CURNN	majority	93.83	91.51	0.0586	92.45	90.56	94.93
eXpose, PDRCNN, XGBoost, CURNN	majority	93.25	91.47	0.1001	94.25	88.68	94.93
PDRCNN, XGBoost, CURNN	majority	93.42	91.11	0.0985	92.48	89.73	94.72
eXpose, PDRCNN, XGBoost	majority	93.63	91.08	0.0832	91.69	90.47	94.69
eXpose, PDRCNN, CURNN	majority	93.59	91.08	0.0638	91.82	90.34	94.69
eXpose, CURNN	majority	92.75	90.96	0.02071	94.27	87.65	94.66
PDRCNN, CURNN	majority	92.11	90.40	0.0614	94.52	86.28	94.35
eXpose, PDRCNN	majority	92.33	90.32	0.04451	93.54	87.09	94.31
eXpose, CURNN	or	93.43	89.22	0.0207	85.61	92.83	93.37
PDRCNN, CURNN	or	93.14	89.12	0.0604	86.41	91.82	93.39
XGBoost, CURNN	or	93.28	89.04	0.056	85.54	92.54	93.28
eXpose, XGBoost	majority	89.99	88.34	0.0402	94.81	81.87	93.22
eXpose, PDRCNN	or	92.96	88.29	0.0445	83.84	92.74	92.73
XGBoost, CURNN	majority	89.66	88.07	0.0556	95.01	81.13	93.07
PDRCNN, XGBoost	or	92.79	88.06	0.0798	83.59	92.53	92.59
eXpose, PDRCNN, CURNN	or	92.97	87.97	0.0628	82.42	93.52	92.40
eXpose, XGBoost	or	92.98	87.88	0.0401	82.47	93.29	92.42
PDRCNN, XGBoost, CURNN	or	92.89	87.81	0.0981	82.04	93.58	92.27
eXpose, XGBoost, CURNN	or	92.93	87.66	0.0584	81.15	94.17	92.07
PDRCNN, XGBoost	majority	89.25	87.50	0.07998	94.49	80.50	92.77
CURNN, FFNN	majority	88.40	87.37	30.9519	96.71	78.03	92.61
eXpose, PDRCNN, XGBoost	or	92.55	86.97	0.0822	79.77	94.16	91.53
PDRCNN, FFNN	majority	88.07	86.92	30.9752	96.36	77.48	92.38
CURNN, FFNN	or	92.94	86.87	30.9517	76.84	96.90	90.89
eXpose, PDRCNN, XGBoost, CURNN	or	92.45	86.67	0.1005	78.82	94.52	91.22
eXpose, FFNN	or	92.33	85.85	30.9358	74.53	97.17	89.90
XGBoost, FFNN	or	92.05	85.57	30.9711	74.80	96.33	89.86
PDRCNN, FFNN	or	92.38	85.47	30.9755	74.14	96.79	90.13
PDRCNN, CURNN, FFNN	or	92.09	85.46	30.9938	73.65	97.26	89.50
eXpose, CURNN, FFNN	or	91.98	85.27	30.9541	73.11	97.43	89.27
XGBoost, CURNN, FFNN	or	91.95	85.23	30.9894	73.07	97.39	89.24
XGBoost, FFNN	majority	86.08	84.90	30.9721	96.27	73.53	91.26
eXpose, PDRCNN, FFNN	or	91.59	84.71	30.9779	71.99	97.43	88.72
PDRCNN, XGBoost, FFNN	or	91.52	84.61	31.0132	71.83	97.39	88.63
eXpose, XGBoost, FFNN	or	91.32	84.31	30.9735	71.07	97.55	88.27
eXpose, PDRCNN, CURNN, FFNN	or	91.31	84.29	30.9962	71.03	97.55	88.25
PDRCNN, XGBoost, CURNN, FFNN	or	91.21	84.16	31.0315	70.77	97.55	88.12
eXpose, XGBoost, CURNN, FFNN	or	91.04	83.91	30.9918	70.16	97.66	87.81
eXpose, PDRCNN, XGBoost, FFNN	or	90.70	83.46	31.0156	69.25	97.66	87.33
All Detectors Combined	or	90.47	83.16	31.0339	68.59	97.72	86.98

## Appendix D. Transfer Theorem and Algorithm

### Appendix D.1. Density Function-based Security Transfer

Let  $K \in \mathbb{N} \setminus \{1\}$  and  $\{d_n^k\}_{k=0}^K \subseteq \mathbb{R}$  be a strictly increase sequence, such that  $T_n = [d_n^0, d_n^K]$  is an interval in  $\mathbb{R}$ . In our method,  $d_n^K$  is the  $s$ -percentile of the dataset  $D_n$ , where  $s \in (0, 1]$ .

Let  $\{L_n^i\}_{i=1}^K$  be a partition of  $T_n$ , such that  $\forall i = 1, 2, \dots, K$ , each  $L_n^i = [d_n^{i-1}, d_n^i]$  represents the  $i$ -th interval of the  $i$ -th case monotonic-increasing function  $\{C_n^i(t)\}_{i=1}^K$ . Thus, the function  $C_n(t)$  is defined as follows:

$$C_n(t) = \min \left\{ \sum_{i=1}^K \mathbf{I}_{L_n^i}(t) C_n^i(t), u \right\} \quad (\text{D.1})$$

where  $\forall i = 1, 2, \dots, K$ ,  $C_n^i(t)$  is elementary and monotonic-increasing in  $L_n^i$ , and  $\mathbf{I}_B(t)$  is the indicator function of the set  $B \subseteq \mathbb{R}$ , which is defined as follows:

$$\mathbf{I}_B(t) = \begin{cases} 1, & t \in B \\ 0, & t \notin B \end{cases} \quad (\text{D.2})$$

Note, we require that  $\forall m = 1, 2, \dots, K - 1$ ,  $C_n^m(d_n^m) = C_n^{m+1}(d_n^m)$ , and also define a constant  $u = C_n^K(d_n^K)$  to ensure the continuity of  $C_n(t)$ .

For a source domain  $n = n_1$  with dataset  $D_{n_1}$  and partitions  $\{L_{n_1}^i\}_{i=1}^K$ , and for a destination domain  $n = n_2 \neq n_1$  with dataset  $D_{n_2}$  and partitions  $\{L_{n_2}^i\}_{i=1}^K$ , we require a proportional difference between the derivatives of each  $i$ -th case function, such that  $C_{n_2}^i(t) \in \Theta(C_{n_1}^i(t))$ .

Next, we define a linear function  $g : L_{n_2}^i \rightarrow L_{n_1}^i$  as follows:

$$g_{n_2 \rightarrow n_1}^i(t) = d_{n_1}^{i-1} + \frac{(d_{n_1}^i - d_{n_1}^{i-1})(t - d_{n_2}^{i-1})}{d_{n_2}^i - d_{n_2}^{i-1}} \quad (\text{D.3})$$

Such that,  $\forall i = 1, 2, \dots, K$ ,  $C_{n_2}^i(t)$  is a composition of  $C_{n_1}^i(t)$  and linear function  $g_{n_2 \rightarrow n_1}^i(t)$  as follows:

$$C_{n_2}^i(t) = C_{n_1}^i(g_{n_2 \rightarrow n_1}^i(t)) \quad (\text{D.4})$$



Next, we define a continuous random variable  $X_n$  with the probability density function (i.e., PDF) as follows:

$$f_{X_n}(t) = \begin{cases} \frac{C_n(t)}{k_n} & , t \in T_n \\ 0 & , \text{otherwise} \end{cases} \quad (\text{D.5})$$

where  $k_n$  is defined as follows:

$$k_n = \int_{T_n} C_n(t) dt = \sum_{i=1}^K \int_{L_n^i} C_n^i(t) dt \quad (\text{D.6})$$

Equation D.6, enables us to ensure that the properties of  $f_{X_n}(t)$  are those of a PDF.

Next, we define a discrete random variable  $Y_n$  as follows:

$$Y_n = \sum_{i=1}^K (i-1) \mathbf{I}_{L_n^i}(X_n) = \sum_{i=2}^K (i-1) \mathbf{I}_{L_n^i}(X_n) \quad (\text{D.7})$$

Such that  $Y_n \in \{0, 1, \dots, K-1\}$ .

Because  $Y_n$  is a discrete random variable, we can create a vectorized representation of the probability mass function  $P_{Y_n} \in [0, 1]^K$ , where the  $i$ -th entry is defined as follows:

$$\mathbb{P}(Y_n = i-1) = \int_{L_n^i} f_{X_n}(t) dt \quad (\text{D.8})$$

where  $i = 1, 2, \dots, K$ .

Note, from equations D.5-D.8, we derive the following:

$$\begin{aligned} \sum_{i=1}^K \mathbb{P}(Y_n = i-1) &= \sum_{i=1}^K \int_{L_n^i} f_{X_n}(t) dt \\ &= \int_{\cup_{i=1}^K L_n^i} f_{X_n}(t) dt = \int_{T_n} f_{X_n}(t) dt = 1 \end{aligned} \quad (\text{D.9})$$

where  $i = 1, 2, \dots, K$ .

Based on equation D.8, we define the likelihood ratios' vector  $\beta_n = (\beta_n^1, \beta_n^2, \dots, \beta_n^K)^T \in \mathbb{R}^K$ , where the  $i$ -th entry is defined as follows:

$$\beta_n^i = \frac{\mathbb{P}(Y_n = i - 1)}{\mathbb{P}(Y_n = 0)} = \frac{\int_{L_n^i} f_{X_n}(t) dt}{\int_{L_n^1} f_{X_n}(t) dt} = \frac{\int_{L_n^i} C_n^i(t) dt}{\int_{L_n^1} C_n^1(t) dt} \quad (\text{D.10})$$

where  $i = 1, 2, \dots, K$ .

Based on equations D.9 and D.10, we derive the following:

$$\mathbb{P}(Y_n = i - 1) = \frac{\beta_n^i}{1_K^T \beta_n} \quad (\text{D.11})$$

where  $i = 1, 2, \dots, K$  and  $1_K \in \mathbb{R}^K$  is a column vector, which all his entries are 1.

For the datasets  $D_{n_1}$  and  $D_{n_2}$ , the Kullback–Leibler (i.e., KL) divergence [31] between  $Y_{n_1}$  and  $Y_{n_2}$  is defined as follows:

$$D_{KL}(Y_{n_1} \| Y_{n_2}) = \sum_{y=0}^{K-1} \mathbb{P}(Y_{n_1} = y) \log_{10} \left( \frac{\mathbb{P}(Y_{n_1} = y)}{\mathbb{P}(Y_{n_2} = y)} \right) \quad (\text{D.12})$$

To require that the density of  $D_{n_2}$  is similar to  $D_{n_1}$ , and since the KL metric is not symmetrical [32], we require that:

$$0 < \frac{D_{KL}(Y_{n_1} \| Y_{n_2}) + D_{KL}(Y_{n_2} \| Y_{n_1})}{2} < \varepsilon \quad (\text{D.13})$$

where  $\varepsilon$  is hyper-parameter tolerance that decide how much the distributions could differ. Since the KL measure is a convex function[49], and its global minimum is 0 (i.e., where distributions  $Y_{n_1}, Y_{n_2}$  are the same, by Gibbs' inequality[50]), we require that the inequality would be greater than 0. This requirement is derived from the assumption that the distributions  $Y_{n_1}, Y_{n_2}$  are not the same (i.e., the domains are in fact different). Note, for destination dataset  $n = n_2$ , the function  $C_{n_2}$  depends on  $K + 1$  variables:  $\{d_{n_2}^k\}_{k=0}^K$ , and the only  $K - 1$  variables we could find are  $\{\beta_{n_2}^k\}_{k=2}^{K-1}$  (i.e.,  $\beta_{n_2}^1$  is always 1), we require that  $T_{n_2} = [d_{n_2}^0, d_{n_2}^K] \subseteq \mathbb{R}$  is known (i.e.,  $d_{n_2}^0, d_{n_2}^K$  are known). The algorithm to the presented above is shown below.

---

**Algorithm 1** Density Function-based Security Transfer From S to D
 

---

1: **input:**

$$K \in \mathbb{N} \setminus \{1\}$$

$\{d_S^k\}_{k=0}^K \in \mathbb{R}$  ; strictly increase sequence.

$d_D^0, d_D^k$  ; subset – strictly increase sequence  $\{d_D^k\}_{k=0}^K \in \mathbb{R}$ .

$d_S^K, d_D^K$  ; s-percentiles of datasets  $S, D$ , respectively.

$$T_S = [d_S^0, d_S^K], T_D = [d_D^0, d_D^K].$$

$\forall i = 1, 2, \dots, K$ , monotonic elementary function  $C_S^i$ :

$$C_S^i : [d_S^{i-1}, d_S^i] \rightarrow \mathbb{R}_{\geq 0}, (C_S^i)' : [d_S^{i-1}, d_S^i] \rightarrow \mathbb{R}_{\geq 0}.$$

$$\forall m = 1, 2, \dots, K-1, C_S^m(d_S^m) = C_S^{m+1}(d_S^m).$$

$\varepsilon > 0$  ; distribution tolerance rate.

$\alpha > 0$  ; learning rate.

2: **for**  $i = 1, 2, \dots, K$

$$L_S^k = [d_S^{k-1}, d_S^k]$$

$$L_D^k = [d_D^{k-1}, d_D^k]$$

$$C_D^i(t; d_D^{i-1}, d_D^i) = C_S \left( d_S^{i-1} + \frac{(d_S^i - d_S^{i-1})(t - d_D^{i-1})}{d_D^i - d_D^{i-1}} \right)$$

$$\beta_S^i = \int_{L_S^i} C_S^i(t) dt \left( \int_{L_S^1} C_S^1(t) dt \right)^{-1}$$

**end for**

3: **define:**

$$u_S = C_S^K(d_S^K), u_D = C_D^K(d_D^K)$$

$$C_S(t) = \min \left\{ \sum_{i=1}^K \mathbf{I}_{L_S^i}(t) C_S^i(t), u_S \right\}$$

$$C_D(t) = \min \left\{ \sum_{i=1}^K \mathbf{I}_{L_D^i}(t) C_D^i(t), u_D \right\}$$

$$\beta_S = (1, \beta_S^2, \dots, \beta_S^K)^T \in \mathbb{R}_{\geq 0}^K$$

Sample  $\theta = (\theta^1, \theta^2, \dots, \theta^{K-1})^T \in \mathbb{R}_{> 0}^{K-1}$  randomly.

$$\psi = (1, \theta^1, \theta^2, \dots, \theta^{K-1})^T = (1, \theta^T)^T \in \mathbb{R}_{> 0}^K$$

Random vars. :  $Y_S, Y_D \in \{0, 1, \dots, K-1\}$  w.p.:

$$P_{Y_S} = (1_K^T \beta_S)^{-1} \beta_S, P_{Y_D} = (1_K^T \psi)^{-1} \psi$$

$$h(\psi; \beta_S) = \frac{1}{2} (D_{KL}(Y_S \| Y_D) + D_{KL}(Y_D \| Y_S))$$

4: **while**  $h(\psi; \beta_S) \geq \varepsilon$

$$\theta \leftarrow \theta - \alpha \nabla_{\theta} h(\psi; \beta_S)$$

$$\psi \leftarrow (1, \theta^T)^T$$

**end while**

5:  $\beta_D = \psi$

6: **for**  $m = 1, \dots, K-1$

derive  $d_D^m$  from the equation:

$$\sum_{i=m+1}^K \beta_D^i = \int_{d_D^m}^{d_D^K} C_D(t) dt \left( \int_{L_D^1} C_D^1(t) dt \right)^{-1}$$

**end for**

7: **return**  $C_D(t)$

---